

A diagnosis scheme for topological degeneracies at high-symmetry momenta

Tiantian Zhang,^{1,2,3,*} Ling Lu,¹ Shuichi Murakami,² Zhong Fang,^{1,4} Hongming Weng,^{1,4,†} and Chen Fang^{1,5,‡}

¹*Institute of Physics, Chinese Academy of Sciences/Beijing National Laboratory for Condensed Matter Physics, Beijing 100190, China*

²*Department of Physics, Tokyo Institute of Technology, Ookayama, Meguro-ku, Tokyo 152-8551, Japan*

³*Tokodai Institute for Element Strategy, Tokyo Institute of Technology, Nagatsuta, Midori-ku, Yokohama, Kanagawa 226-8503, Japan*

⁴*Collaborative Innovation Center of Quantum Matter, Beijing, 100084, China*

⁵*CAS Center for Excellence in Topological Quantum Computation, Beijing 100190, China*

Theories of symmetry-based indicators and topological quantum chemistry, while powerful in diagnosing gapped topological materials, cannot be directly applied to diagnosing band degeneracies at high-symmetry momenta due to the violation of the compatibility conditions. Here we design a recursive protocol that utilizes indicators of maximal subgroups to infer the topological nature of band degeneracies at high-symmetry lines. For demonstration, the method is used to predict the existence of iso-energy Weyl points and a node-line cage, respectively, in the phonon bands of In_2Te and ZrSiO .

Introduction Theories of symmetry-based topological indicators[1] and topological quantum chemistry[2] are useful in diagnosing topological gapped materials such as topological insulators[3–6] and topological crystalline insulators[7–9]. The application of the theory presupposes that along high-symmetry lines in the Brillouin zone (BZ), the conduction and the valence bands do not cross each other, or, put in a formal way, the valence bands satisfy the compatibility conditions, as shown in Fig. 1(a). When these conditions are violated for any pair of high-symmetry points, one only knows that the system is gapless, *i.e.*, having band crossing between the conduction and the valence bands, as shown in Fig. 1(b). Aside from the existence, the method does not yield further information on the band topology associated with these degeneracies.

The importance of such information, however, is highlighted in the research of topological semimetals, such as Weyl semimetals[10–14], Dirac semimetals[15–18], and nodal-line semimetals[19, 20]. The nontrivial topology of band degeneracies in some of these materials leads to unique surface states having “Fermi arcs”[21–24] as well as an anomalous bulk transport phenomenon known as the “quantum anomaly”[25–29]. Topologically nontrivial band degeneracies appear not only in electronic bands but are also predicted and observed in the bands of bosons such as photons[30–33], phonons[34–48], and magnons[49, 50].

In this Letter, we develop a routine for topological-diagnosing band degeneracies located along high-symmetry lines in BZ, especially for orthogonal Hamiltonians[51–53]. Given a band structure that violates the compatibility conditions of some space group G , we first identify, through a “tree-search” process, the maximum subgroup $H \subset G$, such that the compatibility conditions of H are satisfied, and then compute the symmetry-based indicators with respect to H . The values of these subgroup indicators then reveal partial in-

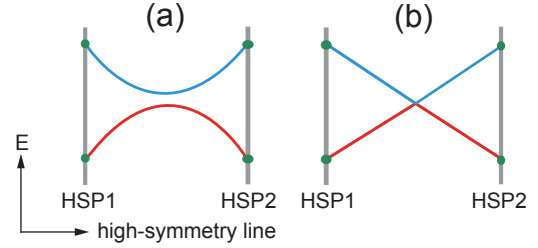


FIG. 1. Two different kinds of band structure along a high-symmetry line. The red line represents the valence band, and the blue line represents the conduction band. HSP1 and HSP2 represent two different high-symmetry point in the Brillouin zone. The band structure in (a) satisfies the compatibility condition, while (b) does not.

formation on topological invariants of the band degeneracies protected by G , which has not been discussed in detail before[4, 8, 9]. For example, the lowest six phonon bands of In_2Te violate the compatibility conditions of #216. Fig. 2 shows all subgroups of space group #216, from which we identify #82 as the maximum subgroup that has nontrivial indicator group (\mathbb{Z}_2) and satisfies the compatibility condition at the same time. We then compute the \mathbb{Z}_2 -indicator for #82 and find $z_2 = 1$, which by Ref.[4] ensures that the band degeneracies between the sixth and the seventh band are Weyl points of equal energy. We also apply the method to the phonon bands of ZrSiO and show the presence of a “nodal cage” in its band structure.

Flowchart for the recursive algorithm The diagnosing process for topological degeneracies at high-symmetry momenta is summarized in Fig. 3, which consists of five steps. In step I, symmetry data, *i.e.*, irreducible representation, at a given list of high-symmetry momenta should

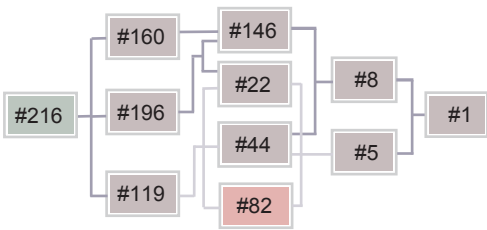


FIG. 2. Tree-search process for #216. #82 is the maximum subgroup which has a nontrivial symmetry-based indicator and satisfies compatibility condition.

be calculated by first-principle calculations. In step II, analyze if two conditions, *i.e.*, the nontrivial-symmetry-based-indicator-group condition (INDC) and compatibility condition (CC) are satisfied by the space group and the symmetry data, respectively. If the space group G has a nontrivial symmetry-based indicator group, and the symmetry data satisfies CC, then we can calculate the symmetry-based indicator directly by Ref.[4] to get the information of topological band degeneracies at generic momenta in the BZ. If space group G does not have a nontrivial symmetry-based indicator group, but the symmetry data satisfies CC, then the system is in a “trivial” state. (Here “trivial” means the symmetry data is that of an atomic insulator.) In other cases, CC is not satisfied, *i.e.*, band degeneracies will exist at high-symmetry momenta, so we should use a new method to diagnose the information for band crossings in the BZ. In Step III, we find all the maximal subgroups of G , and choose one H from this set, and test if the INDC and CC are satisfied: if the answer is YY, we proceed to step IV; if the answer is YN or NN, we replace G by H and repeat step III; if the answer is NY, we replace G by another one of its maximal subgroup $H' \neq H$ and repeat step III until all the maximal subgroups have been exhausted. In step IV, we should use the symmetry-based indicator formula of H to diagnose the topological degeneracy information of space group G , no matter the indicator is zero or not. After step IV, replace G by another one of its subgroups $H' \neq H$ unless all maximal subgroups are exhausted. In the last step, the indicator of subgroup H can tell us the information of topological degeneracies at high-symmetry momenta, such as types, configuration, positions, and topological charge for the topological degeneracies in the BZ. If the process never reaches step IV but stops when all the maximal subgroups of G are considered, we conclude that the nodes cannot be further diagnosed by eigenvalues at all (non-diagnosable). After the process, each band nodes protected by G are to be found either as non-diagnosable, or as having a list of subgroups with corresponding indicators, which carry topological information on these nodes.

Figure. 3 also list two materials for the demonstration of our recursive algorithm in phononic systems. (a) is an example of In_2Te , which has a noncentrosymmetric structure and isoenergy Weyl points in the phonon spectra. (b) is an example of ZrSiO , which has a centrosymmetric structure and nodal cage band degeneracies in the phonon spectrum. Both of the cases break CC in step II.

Diagnosing process for In_2Te In_2Te belongs to a \mathcal{P} -broken space group $F\bar{4}3m$ (#216)[54], as shown in Fig.4(a). The band crossing at around 3.22THz indicates that CC is broken along $X - W$ direction when the number of bands is 6, as shown in Fig. 4(e). In the following, we will get the complete information for the band crossing at around 3.22THz by using the diagnosing method shown in Fig. 3.

After obtaining symmetry data for #216 in step I[55, 56], we notice that CC for #216 is not satisfied along $X - W$ direction, which is not a surprise because of the band crossing in phonon spectra. However, there is not a nontrivial indicator for space group #216 in step II. Therefore in step III, we map each irreducible representation from #216 to #82 ($I\bar{4}$), which is the maximum subgroup having a nontrivial indicator \mathbb{Z}_2 and satisfying CC. In step IV, we calculate the topological invariant of subgroup #82 and get a nonzero indicator $z_2 = 1$, which indicates that there will be 4 *mod* 8 Weyl points on the $k_z = 0$ plane (which is also $k_3 = 0$ plane). In the following, we will provide an intuitive perspective to understand how to get the complete information for the topological degeneracies at high-symmetry momenta for #216 from the indicator of subgroup #82.

Figure. 4(c) shows the BZ for space group #82, which has a similar shape with the one for #216 shown in Fig. 4(b). Since there are two pieces of plane for $k_z = 0$ plane in Fig. 4(b), we can rebuild the BZ by dividing the blue quadrilateral plane into four pieces and fill them into the pink plane separately to get a new quadrilateral $k_1 = 0$ plane. In this case, high-symmetry point M_1 in the old BZ is M_2 in the new BZ. Since there are 4 *mod* 8 Weyl points on the $k_1 = 0$ plane, shown by red and green dots in Fig. 4(c), we find that there will be 12 *mod* 24 Weyl points in the BZ after considering all the symmetry operators of #216, especially C_3 symmetry around (111) direction. A detailed calculation confirms that there are 12 robust Weyl points related to each other by symmetries at around 3.22THz, confined in in $k_1 = 0$, $k_2 = 0$, and $k_3 = 0$ planes.

Surface states for the Weyl points in In_2Te Fig. 4(d) show the positions of 12 Weyl points in the BZ, where green dots represent left-hand Weyl points with Chern number of -1 and red dots represent right-hand Weyl points with Chern number of $+1$. Among those six pairs of Weyl points, W_1 and W_2 have opposite chirality, which are related by mirror symmetry m_{011} . The Weyl pairs $W_{1,2}$, $W_{5,6}$, and $W_{9,10}$ are related to each other by C_3 rotation symmetry along (111) direction, and those

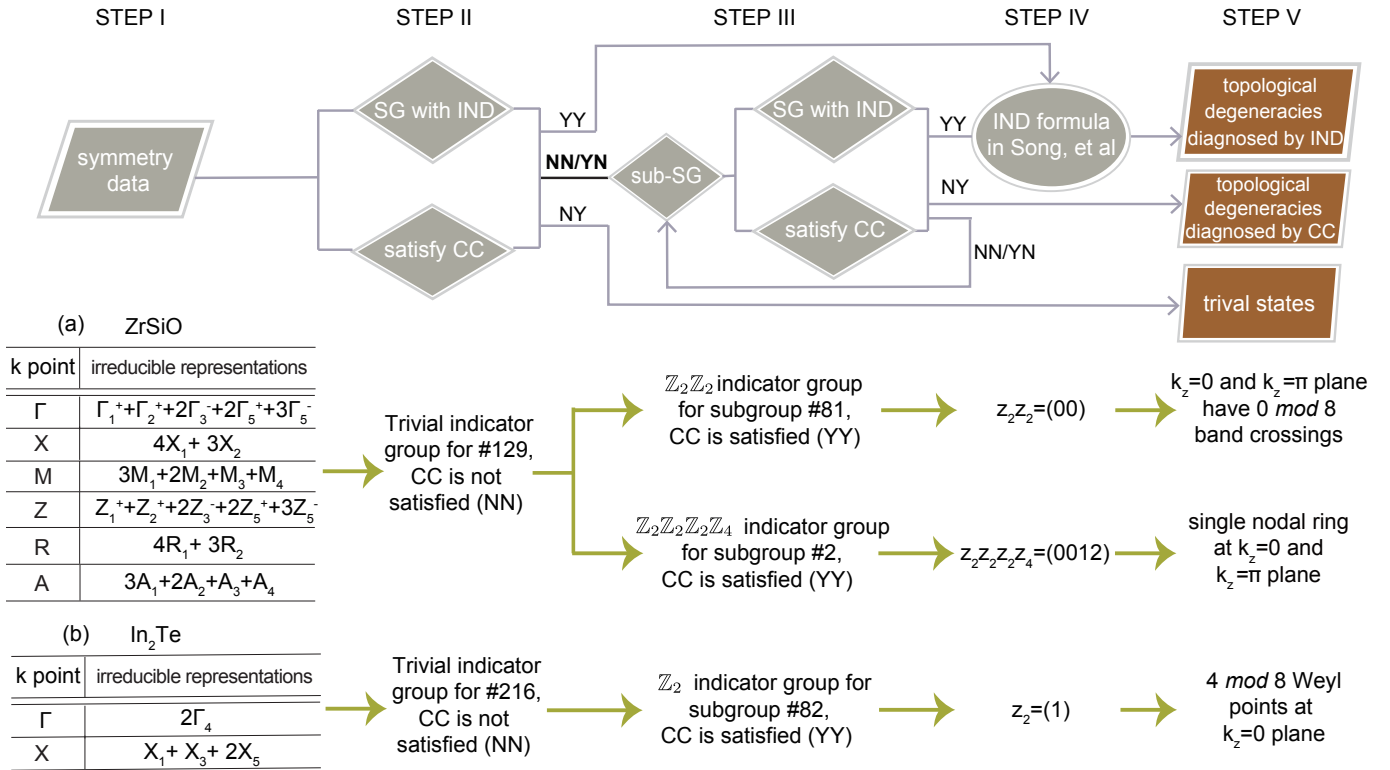


FIG. 3. Calculation steps for diagnosing topological degeneracies at high-symmetry momenta. SG=space group, IND=indicator, CC=compatibility condition, N=No, Y=Yes. First of all, symmetry data should be obtained by first-principle calculations, and fed into the next step. Secondly, check whether the space group G has a nontrivial indicator and the symmetry data satisfies compatibility conditions. If both the answers are yes, we can use the symmetry data to calculate the indicator directly and get the information of topological degeneracies at generic momenta for AI class systems. If the answers are “NY”, the material is a topologically trivial one. Otherwise, topological degeneracies will exist at high-symmetry momenta, such as high-symmetry points, high-symmetry lines, and high-symmetry planes. To get the complete information of the topological band crossings, we should find a maximum subgroup H in step III, which has a nontrivial symmetry-based indicator group and satisfies compatibility condition at the same time. After calculating the symmetry-based indicator for H in step IV, we can get the information of topological degeneracies for space group G . However, if we can not find a subgroup H in step III, then the topological degeneracies only can be diagnosed by compatibility condition. (a) In_2Te (b) ZrSiO are two examples for demonstrating our diagnosis scheme for AI class systems.

three pairs of Weyl points are related with the remaining three pairs of Weyl points by \mathcal{T} . Local density of states (LDOS) on the $(11\bar{1})$ surface is shown in Fig. 4(f), plotted along the surface momentum lines $\bar{K} - \bar{\Gamma} - \bar{M} - \bar{K}$. The surface arcs are clearly seen at around 3.22THz.

Here, we note that there are another 12 Weyl nodes at around 2.58THz, with the same indicator $z_2 = 1$. Surface states and surface arcs for the 12 Weyl nodes at around 2.58THz are discussed in the supplementary materials.

Diagnosis process for ZrSiO ZrSiO has a centrosymmetric structure with space group $P4/nmm$ (#129)[57], as shown in Fig. 5(a). ZrSiO is a nodal line semimetal for electronic structures when spin-orbit coupling is ignored[19] and features the same topological properties for phonon spectra. Figure. 5(c) shows the phonon bands for ZrSiO , which have several band crossings at around 13THz along several high-symmetry lines. We will discuss what they are, and whether they are topological

protected in the following.

After obtaining the symmetry data by density-function perturbation theory in step I, we find out that they do not satisfy the CC along $\Gamma - X$, $\Gamma - M$, $Z - A$, and $Z - R$ directions when the occupied bands is 14 in step II. Violation of CC indicates that a band degeneracy will exist between the 14th and 15th band at those four high-symmetry lines, which also means we can use the recursive algorithm to figure out the complete topological information for the degeneracies. In step III, we find that the maximum subgroup having a nontrivial symmetry-based indicator for #129 is #85. However, CC is not satisfied for #85. Thus, we need to proceed the recursive process to check the subgroups with lower symmetries. After iterating several times, we get two maximum subgroups having a nontrivial indicator and satisfying CC,

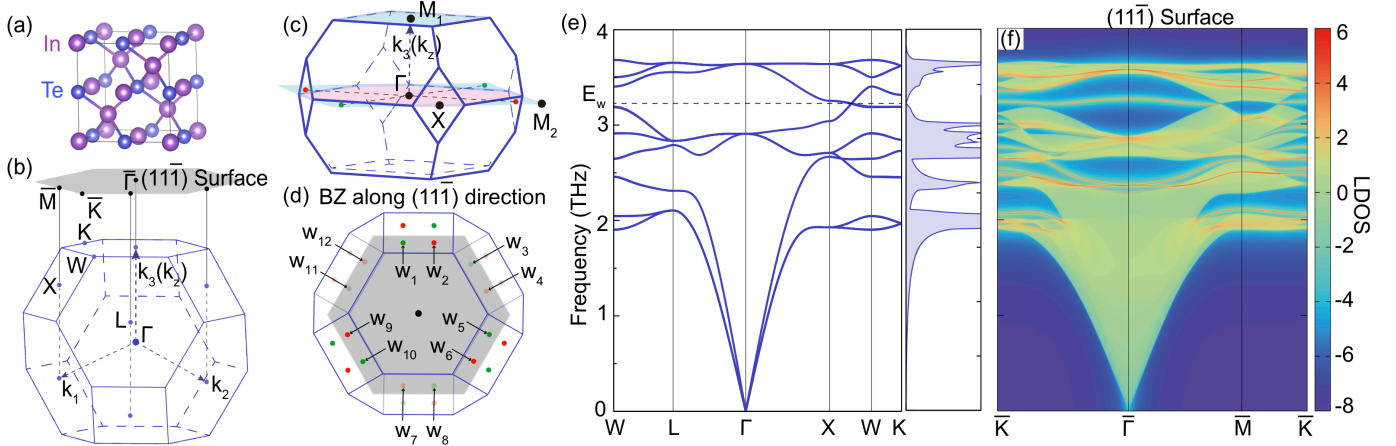


FIG. 4. (a) Crystal structure for In_2Te , (b) Brillouin zone and surface Brillouin zone along $(11\bar{1})$ direction for #216. (c) Brillouin zone for #82. (d) Distribution for Weyl points in the Brillouin zone, where green dots represent Weyl points with Chern number of -1 and red dots represent Weyl points with Chern number of $+1$. (e) Phonon spectra for In_2Te and (f) is the surface state along $(11\bar{1})$ direction.

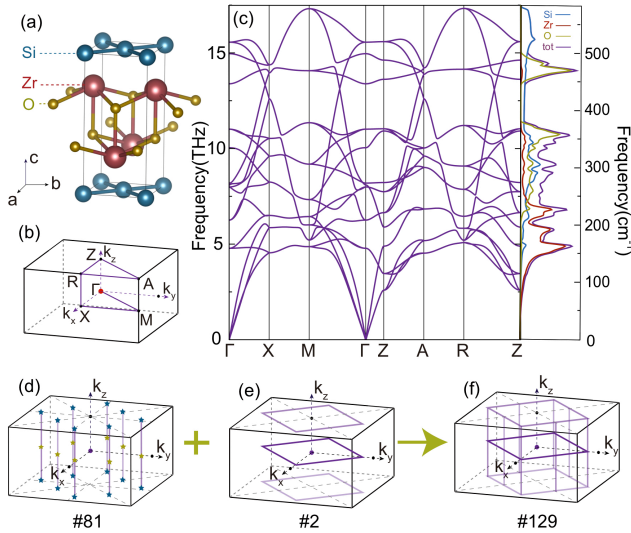


FIG. 5. (a) Crystal structure, (b) Brillouin zone, and (c) phonon spectra for ZrSiO . (d-f) are the configurations for node-line degeneracies in Brillouin zone. All the nodal lines carry a quantized π Berry phase.

which are #81 and #2. #81 and #2 belong to different “tree branches”, which means that neither of them is a subgroup of the other one.

The indicator group for #81 is $\mathbb{Z}_2 \times \mathbb{Z}_2$, and the corresponding topological invariants for phonons in ZrSiO are (00). Even though the topological invariants are zero, they can still tell us that there will be $0 \bmod 8$ band crossings at both $k_z = 0$ plane and $k_z = \pi$ plane. As shown

in 5(d), band crossings are marked by pentagrams. Since $(PT)^2 = 1$ in ZrSiO , all the band crossings must belong to nodal lines/rings. Therefore a possible configuration for the band degeneracies in ZrSiO diagnosed by #81 is $0 \bmod 8$ nodal lines crossing both $k_z = 0$ plane and $k_z = \pi$ plane along (001) direction, as shown in Fig. 5(d).

The indicator group for #2 is $\mathbb{Z}_2 \times \mathbb{Z}_2 \times \mathbb{Z}_2 \times \mathbb{Z}_4$, and the corresponding topological invariants are (0012) for phonons in ZrSiO . Those nonzero indicators tell us a new configuration for the topological degeneracies in BZ, and we offer two different perspectives to understand it. (i) Because indicator groups are Abelian groups, indicators satisfy the sum rule. Thus (0012) can be written as (0001)+(0011), which indicates a single nodal ring around Γ and Z point by Ref.[4], respectively. M_z symmetry in ZrSiO will restrict those two nodal rings in the $k_z = 0$ and $k_z = \pi$ plane, which corresponds to the configuration shown in Fig. 5(e). (ii) $z_2 = 1$ and $z_4 = 2$ indicate that any curved surface in the BZ passing Γ , X , and M point (or R , A , and Z point) will be crossed by nodal lines $2 \bmod 4$ times. Therefore one possible configuration is one nodal ring lying on the $k_z = 0$ and $k_z = \pi$ plane respectively, which also matches Fig. 5(e) well.

In the last step, we can get the complete configuration for topological degeneracies in BZ by combining the indicators of subgroup #81 and #2. Further calculations show that there are 8 nodal lines and 2 nodal rings in the BZ, *i.e.*, node-cage degeneracies shown in Fig. 5(f), which perfectly matches the diagnosis. Indicators from those two subgroups also tell us that each nodal line/ring in ZrSiO carries a π Berry phase, and zero monopole charge.

Surface states for nodal lines/rings are in a drum-head shape, but it is not easy to observe them experimentally for being easily covered by the bulk dispersions.

Conclusion We designed a recursive algorithm for diagnosing the complete information of topological degeneracies locating at high-symmetry momenta by using the indicators of maximum subgroups. This recursive algorithm can be used in any systems with $\mathcal{T}^2 = 1$ and compensates for the shortcomings of the previous method, which can only be used in systems satisfying compatibility conditions, *i.e.*, no band degeneracies at high-symmetry momenta. In two examples for phonon bands, *i.e.*, In_2Te and ZrSiO , we diagnosed all the topological degeneracies in the BZ successfully, which verifies the effectiveness of the diagnosing method.

* zhang.t.ac@m.titech.ac.jp

† hmweng@iphy.ac.cn

‡ cfang@iphy.ac.cn

- [1] Hoi Chun Po, Ashvin Vishwanath, and Haruki Watanabe. Symmetry-based indicators of band topology in the 230 space groups. *Nature Communications*, 8(1):50, 2017.
- [2] Barry Bradlyn, L Elcoro, Jennifer Cano, MG Vergniory, Zhijun Wang, C Felser, MI Aroyo, and B Andrei Bernevig. Topological quantum chemistry. *Nature*, 547(7663):298, 2017.
- [3] Zhida Song, Tiantian Zhang, Zhong Fang, and Chen Fang. Quantitative mappings between symmetry and topology in solids. *Nature communications*, 9(1):3530, 2018.
- [4] Zhida Song, Tiantian Zhang, and Chen Fang. Diagnosis for nonmagnetic topological semimetals in the absence of spin-orbital coupling. *Physical Review X*, 8(3):031069, 2018.
- [5] Xiao-Liang Qi and Shou-Cheng Zhang. Topological insulators and superconductors. *Reviews of Modern Physics*, 83(4):1057, 2011.
- [6] CL Kane and TC Lubensky. Topological boundary modes in isostatic lattices. *Nature Physics*, 10(1):39–45, 2014.
- [7] Tiantian Zhang, Yi Jiang, Zhida Song, He Huang, Yuqing He, Zhong Fang, Hongming Weng, and Chen Fang. Catalogue of topological electronic materials. *Nature*, 566(7745):475, 2019.
- [8] MG Vergniory, L Elcoro, Claudia Felser, Nicolas Regnault, B Andrei Bernevig, and Zhijun Wang. A complete catalogue of high-quality topological materials. *Nature*, 566(7745):480, 2019.
- [9] Feng Tang, Hoi Chun Po, Ashvin Vishwanath, and Xiangang Wan. Comprehensive search for topological materials using symmetry indicators. *Nature*, 566(7745):486, 2019.
- [10] Hongming Weng, Chen Fang, Zhong Fang, B Andrei Bernevig, and Xi Dai. Weyl semimetal phase in noncentrosymmetric transition-metal monophosphides. *Physical Review X*, 5(1):011029, 2015.
- [11] Chen Fang, Matthew J Gilbert, Xi Dai, and B Andrei Bernevig. Multi-weyl topological semimetals stabilized by point group symmetry. *Physical Review Letters*, 108(26):266802, 2012.
- [12] Gang Xu, Hongming Weng, Zhijun Wang, Xi Dai, and Zhong Fang. Chern semimetal and the quantized anomalous hall effect in HgCr_2Se_4 . *Physical Review Letters*, 107(18):186806, 2011.
- [13] Shin-Ming Huang, Su-Yang Xu, Ilya Belopolski, Chi-Cheng Lee, Guoqing Chang, Tay-Rong Chang, BaoKai Wang, Nasser Alidoust, Guang Bian, Madhab Neupane, et al. New type of Weylsemimetal with quadratic doubleWeylfermions. *Proceedings of the National Academy of Sciences*, 113(5):1180–1185, 2016.
- [14] Barry Bradlyn, Jennifer Cano, Zhijun Wang, MG Vergniory, C Felser, RJ Cava, and B Andrei Bernevig. BeyondDiracandWeylfermions: Unconventional quasiparticles in conventional crystals. *Science*, 353(6299):aaf5037, 2016.
- [15] Zhijun Wang, Hongming Weng, Quansheng Wu, Xi Dai, and Zhong Fang. Three-dimensionalDiracsemimetal and quantum transport in cd_3as_2 . *Phys. Rev. B*, 88:125427, Sep 2013.
- [16] Zhijun Wang, Yan Sun, Xing-Qiu Chen, Cesare Franchini, Gang Xu, Hongming Weng, Xi Dai, and Zhong Fang. Dirac semimetal and topological phase transitions in A_3Bi ($a = \text{Na, K, Rb}$). *Phys. Rev. B*, 85:195320, May 2012.
- [17] ZK Liu, B Zhou, Y Zhang, ZJ Wang, HM Weng, D Prabhakaran, S-K Mo, ZX Shen, Z Fang, X Dai, et al. Discovery of a three-dimensional topologicalDiracsemimetal, na_3bi . *Science*, 343(6173):864–867, 2014.
- [18] R. M. Geilhufe, S. S. Borysov, A. Bouhon, and A. V. Balatsky. Data Mining for Three-Dimensional OrganicDiracMaterials: Focus on Space Group 19. *ArXiv e-prints*, November 2016.
- [19] Qiunan Xu, Zhida Song, Simin Nie, Hongming Weng, Zhong Fang, and Xi Dai. Two-dimensional oxide topological insulator with iron-pnictide superconductor lifeas structure. *Physical Review B*, 92(20):205310, 2015.
- [20] Chen Fang, Hongming Weng, Xi Dai, and Zhong Fang. Topological nodal line semimetals. *Chinese Physics B*, 25(11):117106, 2016.
- [21] BQ Lv, HM Weng, BB Fu, XP Wang, H Miao, J Ma, P Richard, XC Huang, LX Zhao, GF Chen, et al. Experimental discovery ofWeylsemimetal taas. *Physical Review X*, 5(3):031013, 2015.
- [22] Su-Yang Xu, Ilya Belopolski, Nasser Alidoust, Madhab Neupane, Guang Bian, Chenglong Zhang, Raman Sankar, Guoqing Chang, Zhujun Yuan, Chi-Cheng Lee, et al. Discovery of aWeylfermion semimetal and topological fermi arcs. *Science*, 349(6248):613–617, 2015.
- [23] Xiangang Wan, Ari M Turner, Ashvin Vishwanath, and Sergey Y Savrasov. Topological semimetal and fermi-arc surface states in the electronic structure of pyrochlore iridates. *Physical Review B*, 83(20):205101, 2011.
- [24] Wen-Jie Chen, Meng Xiao, and CT Chan. Experimental observation of robust surface states on photonic crystals possessing single and doubleWeylpoints. *arXiv preprint arXiv:1512.04681*, 2015.
- [25] DT Son and BZ Spivak. Chiral anomaly and classical negative magnetoresistance ofWeylmetals. *Physical Review B*, 88(10):104412, 2013.
- [26] Xiaochun Huang, Lingxiao Zhao, Yujia Long, Peipei Wang, Dong Chen, Zhanhai Yang, Hui Liang, Mianqi Xue, Hongming Weng, Zhong Fang, et al. Observa-

- tion of the chiral-anomaly-induced negative magnetoresistance in 3dWeylsemimetal taas. *Physical Review X*, 5(3):031023, 2015.
- [27] Jun Xiong, Satya K Kushwaha, Tian Liang, Jason W Krizan, Max Hirschberger, Wudi Wang, Robert Joseph Cava, and Nai Phuan Ong. Evidence for the chiral anomaly in the Dirac semimetal Na_3Bi . *Science*, 350(6259):413–416, 2015.
- [28] AA Zyuzin and AA Burkov. Topological response in Weyl semimetals and the chiral anomaly. *Physical Review B*, 86(11):115133, 2012.
- [29] Holger Bech Nielsen and Masao Ninomiya. The Adler-Bell-Jackiw anomaly and Weyl fermions in a crystal. *Physics Letters B*, 130(6):389–396, 1983.
- [30] Ling Lu, John D Joannopoulos, and Marin Soljačić. Topological photonics. *Nature Photonics*, 8(11):821, 2014.
- [31] Ling Lu, John D Joannopoulos, and Marin Soljačić. Topological states in photonic systems. *Nature Physics*, 12(7):626, 2016.
- [32] Ling Lu, Zhiyu Wang, Dexin Ye, Lixin Ran, Liang Fu, John D Joannopoulos, and Marin Soljačić. Experimental observation of Weyl points. *Science*, 349(6248):622–624, 2015.
- [33] Wen-Jie Chen, Meng Xiao, and Che Ting Chan. Photonic crystals possessing multiple Weyl points and the experimental observation of robust surface states. *Nature communications*, 7, 2016.
- [34] Tiantian Zhang, Zhida Song, A Alexandradinata, Hongming Weng, Chen Fang, Ling Lu, and Zhong Fang. Double-Weyl phonons in transition-metal monosilicides. *Physical Review Letters*, 120(1):016401, 2018.
- [35] Hu Miao, TT Zhang, Le Wang, Derek Meyers, AH Said, YL Wang, YG Shi, HM Weng, Zhong Fang, and MPM Dean. Observation of double Weyl phonons in parity-breaking fesi. *Physical Review Letters*, 121(3):035302, 2018.
- [36] Romain Fleury, Alexander B Khanikaev, and Andrea Alù. Floquet topological insulators for sound. *Nature Communications*, 7, 2016.
- [37] S Hossein Mousavi, Alexander B Khanikaev, and Zheng Wang. Topologically protected elastic waves in phononic metamaterials. *arXiv preprint arXiv:1507.03002*, 2015.
- [38] Bryan Gin-ge Chen, Nitin Upadhyaya, and Vincenzo Vitelli. Nonlinear conduction via solitons in a topological mechanical insulator. *Proceedings of the National Academy of Sciences*, 111(36):13004–13009, 2014.
- [39] Roman Süssstrunk and Sebastian D Huber. Observation of phononic helical edge states in a mechanical topological insulator. *Science*, 349(6243):47–50, 2015.
- [40] Lisa M Nash, Dustin Kleckner, Alismari Read, Vincenzo Vitelli, Ari M Turner, and William TM Irvine. Topological mechanics of gyroscopic metamaterials. *Proceedings of the National Academy of Sciences*, 112(47):14495–14500, 2015.
- [41] D Zeb Rocklin, Bryan Gin-ge Chen, Martin Falk, Vincenzo Vitelli, and TC Lubensky. Mechanical Weyl modes in topological Maxwell lattices. *Physical Review Letters*, 116(13):135503, 2016.
- [42] Zhaoju Yang, Fei Gao, Xihang Shi, Xiao Lin, Zhen Gao, Yidong Chong, and Baile Zhang. Topological acoustics. *Physical Review Letters*, 114(11):114301, 2015.
- [43] Cheng He, Xu Ni, Hao Ge, Xiao-Chen Sun, Yan-Bin Chen, Ming-Hui Lu, Xiao-Ping Liu, and Yan-Feng Chen. Acoustic topological insulator and robust one-way sound transport. *Nature Physics*, 2016.
- [44] Sebastian D Huber. Topological mechanics. *Nature Physics*, 12(7):621–623, 2016.
- [45] R. Süssstrunk and S. D. Huber. Classification of topological phonons in linear mechanical metamaterials. *Proceedings of the National Academy of Science*, 113:E4767–E4775, August 2016.
- [46] W. Ji and J. Shi. Topological Phonon Modes in A Two-Dimensional Wigner Crystal. *ArXiv e-prints*, December 2016.
- [47] Y. Liu, Y. Xu, S.-C. Zhang, and W. Duan. Topological Phononics and Phonon Diode. *ArXiv e-prints*, June 2016.
- [48] BW Xia, R Wang, ZJ Chen, YJ Zhao, and H Xu. Symmetry-protected ideal type-II Weyl phonons in cdte. *Physical Review Letters*, 123(6):065501, 2019.
- [49] Kangkang Li, Chenyuan Li, Jiangping Hu, Yuan Li, and Chen Fang. Dirac and nodal line magnons in three-dimensional antiferromagnets. *Physical Review Letters*, 119(24):247202, 2017.
- [50] Weiliang Yao, Chenyuan Li, Lichen Wang, Shangjie Xue, Yang Dan, Kazuki Iida, Kazuya Kamazawa, Kangkang Li, Chen Fang, and Yuan Li. Topological spin excitations in a three-dimensional antiferromagnet. *Nature Physics*, 14(10):1011, 2018.
- [51] Andreas P Schnyder, Shinsei Ryu, Akira Furusaki, and Andreas WW Ludwig. Classification of topological insulators and superconductors in three spatial dimensions. *Physical Review B*, 78(19):195125, 2008.
- [52] Ching-Kai Chiu, Jeffrey CY Teo, Andreas P Schnyder, and Shinsei Ryu. Classification of topological quantum matter with symmetries. *Reviews of Modern Physics*, 88(3):035005, 2016.
- [53] Shinsei Ryu, Andreas P Schnyder, Akira Furusaki, and Andreas WW Ludwig. Topological insulators and superconductors: tenfold way and dimensional hierarchy. *New Journal of Physics*, 12(6):065010, 2010.
- [54] G. A. Gamal, A. T. Nagat, M. M. Nassary, and A. M. Abou-Alwafa. Some physical properties of ga_2se single crystals. *Crystal Research and Technology*, 31(3):359–364, 1996.
- [55] Xavier Gonze and Changyol Lee. Dynamical matrices, Born effective charges, dielectric permittivity tensors, and interatomic force constants from density-functional perturbation theory. *Phys. Rev. B*, 55:10355–10368, Apr 1997.
- [56] Georg Kresse and Jürgen Furthmüller. Efficient iterative schemes for ab initio total-energy calculations using a plane-wave basis set. *Physical review B*, 54(16):11169, 1996.
- [57] Hajo Onken, Karl Vierheilg, and Harry Hahn. Über silicid- und germanidchalkogenide des zirkons und hafniums. *Zeitschrift für anorganische und allgemeine Chemie*, 333(4-6):267–279, 1964.